

Open access • Journal Article • DOI:10.1038/NNANO.2012.237

Transferrin-functionalized nanoparticles lose their targeting capabilities when a biomolecule corona adsorbs on the surface — Source link

Anna Salvati, Andrzej S. Pitek, Marco P. Monopoli, Kanlaya Prapainop ...+6 more authors

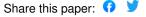
Institutions: University College Dublin

Published on: 01 Feb 2013 - Nature Nanotechnology (Nature Publishing Group)

Topics: Protein Corona, Transferrin receptor and Nanomedicine

Related papers:

- Biomolecular coronas provide the biological identity of nanosized materials
- Rapid formation of plasma protein corona critically affects nanoparticle pathophysiology
- · Nanoparticle size and surface properties determine the protein corona with possible implications for biological impacts
- · Understanding the nanoparticle-protein corona using methods to quantify exchange rates and affinities of proteins for nanoparticles.
- · Understanding biophysicochemical interactions at the nano-bio interface











Research Repository UCD

Provided by the author(s) and University College Dublin Library in accordance with publisher policies. Please cite the published version when available.

Title	Transferrin-functionalized nanoparticles lose their targeting capabilities when a biomolecule corona adsorbs on the surface	
Authors(s)	Salvati, Anna; Pitek, Andrzej S.; Monopoli, Marco P.; Prapainop, Kanlaya; Baldelli Bombelli, Francesca; Hristov, Delyan R.; Kelly, Philip; Åberg, Christoffer; Mahon, Eugene; Dawson, Kenneth A.	
Publication date	2013-01-20	
Publication information	Nature nanotechnology, 8 (2): 137-143	
Publisher	Nature Publishing Group	
Item record/more information	http://hdl.handle.net/10197/4976	
Publisher's version (DOI)	10.1038/nnano.2012.237	

Downloaded 2022-05-30T14:56:30Z

The UCD community has made this article openly available. Please share how this access benefits you. Your story matters! (@ucd_oa)



© Some rights reserved. For more information, please see the item record link above.

Transferrin-functionalized nanoparticles lose their targeting capabilities when a biomolecule corona adsorbs on the surface

Anna Salvati, Andrzej S. Pitek, Marco P. Monopoli, Kanlaya Prapainop, Francesca Baldelli Bombelli, Delyan R. Hristov, Philip M. Kelly, Christoffer Åberg, Eugene Mahon*, Kenneth A. Dawson*

Centre for BioNano Interactions, School of Chemistry and Chemical Biology, UCD Conway Institute for Biomolecular and Biomedical Research, University College Dublin, Belfield, Dublin 4, Ireland

*Corresponding authors:

Prof. Kenneth A. Dawson (Kenneth.A.Dawson@cbni.ucd.ie); Dr. Eugene Mahon (Eugene.Mahon@cbni.ucd.ie)

Centre for BioNano Interactions, School of Chemistry and Chemical Biology, University College Dublin, Belfield, Dublin 4, Ireland

Phone: +353 0 1 716 2459.

Nanoparticles have been proposed as carriers for drugs, genes and therapies to treat various diseases^{1,2}. Many strategies have been developed to "target" nanomaterials to specific or over-expressed receptors in diseased cells, and these typically involve functionalizing the surface of nanoparticles with proteins, antibodies or other biomolecules. Here we show that the targeting ability of such functionalized nanoparticles may disappear when they are placed in a biological environment. Using transferrin-conjugated nanoparticles, we found that proteins in the media can shield transferrin from binding to both its targeted receptors on cells and soluble transferrin receptors. Although nanoparticles continue to enter cells, the targeting specificity of transferrin is lost. Our results suggest that when nanoparticles are placed in a complex biological environment, the interaction with other proteins in the medium and formation of a protein corona^{3,4} can "screen" the targeting molecules on the surface of nanoparticles, and cause loss of specificity in targeting.

The potential of targeting nanomedicines has already been illustrated in practice⁵⁻⁷. Among these general approaches, the role of nanomedicines exploiting active targeting via specific ligands is increasing in prominence⁸⁻¹⁰. These efforts have met with varying success⁵⁻⁷, and it is not always possible to fully explain the different outcomes. Likely, there are several reasons for this^{2,9,11,12}, but certainly there remains a lack of detailed mechanistic information on the link between nanoparticle surface and biological interactions.

Nanoparticles enter most cells by energy dependent processes, some of which not yet fully clarified 13,14. One potential objective of actively targeted nanomedicines is the design of a particle truly specific to a given cell, and which engages only with a specific cellular pathway. Thus, while many nanoparticles enter most cells easily, the overall targeting success depends on the degree of discrimination in nanoparticle uptake; that is, the degree to which nanoparticles are taken up via relevant pathways, and not others. The detailed (*in situ*) structure of the nanoparticle interface with the entire biological environment (both target and biological milieu) is critical in determining this outcome. Here we present methods to evaluate that interface, with serum-rich conditions employed as more representative of *in vivo* studies. For the case of transferrin-targeted particles, some nanoparticle types fail to target the relevant pathway, even though they enter cells efficiently. Furthermore, even nanoparticles that target the relevant pathway may lose that specificity in the presence of a relevant biological milieu. This suggests the future need to design and characterize the nanoparticle-corona interface in more sophisticated ways.

While it is clear that nanoparticle size and shape are key factors for uptake¹⁵⁻¹⁷, current targeting strategies also involve conjugation of biofunctional moieties to nanoparticles in an effort to determine the biological outcomes^{1,2,9,12,18-20}. In some cases this seems successful,

but in others less so (for example targeting moieties can hinder biological barrier penetration^{8,11}). Practical problems include the fact that surface-grafting of biofunctional moieties may disrupt protein structure and function^{21,22}, or constrain its orientation. Polyethylene glycol (PEG) spacers are expected to preserve protein function by moving the targeting moiety from the surface, provide flexibility²³, and reduce non-specific binding of environmental biomolecules²⁴.

As an illustrative example, cancer cell metabolism of iron may lead to over-expression of transferrin receptor $(TfR)^{25}$, making transferrin (Tf, a glycoprotein of 79 kDa that binds TfR at extracellular pH, $K_d = 1-100 \text{ nM})^{26}$, a potential targeting molecule. Previous investigations with Tf-targeted nanoparticles have, sometimes, appeared inconsistent, and problems such as linker stability and protein flexibility have been identified²⁷⁻³⁰.

Here fluorescent silica nanoparticles (SiO₂, 50nm) are prepared by co-condensation of tetraethyl orthosilicate with N-1-(3-trimethoxysilylpropyl)-N'-fluoresceyl thiourea (APTMS-FITC), and modified with maleimide PEG. Human Tf modified with a thiol-PEG linker is conjugated to the pegylated particle to give fluorescent bioconjugates (Scheme 1). A large range of nanoparticles (in excess of 100) with various coupling conditions and PEG lengths has been tested. Notably, chain lengths X and Y are varied, with X = 4 and Y = 8 being found optimal for TfR-mediated uptake (Scheme 1b). Nanoconjugates where Tf is directly coupled at the surface are also prepared. Nanoparticle characterization suggests well defined dispersions after Tf-functionalization for some of these particles (Table 1 and Supplementary Table S1) and immuno dot-blots show recognition of the grafted Tf by anti-Tf antibodies (Supplementary Fig. S1a). While circular dichroism (CD) indicates that Tf structure is largely preserved (Supplementary Fig. S1b), we stress that this alone does not guarantee functional binding, suggesting the need for some of the methods outlined in this paper.

Thus, Differential Centrifugal Sedimentation (DCS) is used to study binding isotherms of nanoparticles to a soluble TfR fragment with preserved functionality. Unlike more conventional light scattering studies, this allows binding to be studied in a wide range of relevant environments. In parallel, RNA interference is used to silence, in this case, the expression of TfR in A549 lung epithelial cells and determine its effect on nanoparticle uptake. We emphasize that the absolute uptake level does not give information on the specificity of these interactions. However, the difference in particle uptake in silenced and non-silenced cells is indicative of the relative contribution made by that pathway. Supplementary Figure S2 shows that in TfR-silenced cells residual TfR is small, and Tf uptake is essentially absent. This silenced cell model is now used to determine the contribution of Tf in the uptake of different nanoparticles.

As a first step, we use simple buffer or serum free medium to test the capacity of different Tf-conjugated nanoparticles to be recognised by TfR. As shown in Supplementary Fig. S3a-d, for a number of nanoparticles with different design, uptake is present in all cases, but does not decrease after TfR silencing. Similarly, the apparent particle size by DCS does not change when the soluble TfR fragment is added (Supplementary Fig. S3e). This indicates absence of interactions of these particles with TfR, which is consistent with the conclusion that uptake is not mediated by TfR.

Optimal design is achieved with Tf-decorated silica nanoparticles with PEG₈ spacers (SiO₂-PEG₈-Tf, as illustrated in Scheme 1b). With these nanoparticles, the apparent particle size by DCS increases with increasing TfR amounts (Fig. 1a-b), and this is reversible in the presence of excess Tf (Supplementary Fig. S4a). This indicates that these nanoparticles are recognised by TfR and bind it, while in the presence of excess Tf, binding is lost due to competition of the free Tf molecules. Furthermore, titration with TfR suggests saturation of receptor binding, which is consistent with roughly 40% of nominal Tf binding sites per particle (Fig. 1b). From these data, we can estimate that roughly 100 TfR molecules are required to saturate one nanoparticle. This is likely an upper limit, because not all of these sites may be accessible on the cell surface. Nevertheless, the potential for multiple receptor binding may be reflected in co-operativity in cellular uptake.

When cells are exposed to these functional Tf-conjugated nanoparticles, confocal imaging shows colocalization of some of the particles with TfR (Fig. 1c). Uptake in TfR-silenced cells is strongly reduced (Fig. 1d). Similarly nanoparticle uptake decreases in the presence of increasing amounts of free Tf, though these competition experiments are less definitive due to potential for non-specific binding of the free Tf to the nanoparticles (Supplementary Fig. S4b).

Overall, this indicates that these nanoparticles are internalised via TfR. Still, silencing also shows that a portion of uptake does not depend on TfR, and this is consistent with the limited colocalization with TfR observed in Fig.1c. Nanoparticle export³¹ appears absent (Fig.1e), at least for time scales comparable to Tf export (shown in Supplementary Fig. S2d), and nanoparticles accumulate in the lysosomes (Fig. 1e).

A variety of other particles with PEG₈-linker has also been examined. Though the efficiency of internalization and uptake kinetics are affected by PEG densities and other details, in all cases the PEG of this size allows us to obtain functional Tf-conjugated nanoparticles internalized via TfR (Supplementary Fig. S5).

As additional examples, we also show that particles with human Tf directly grafted on their surface (Fig. 2a) show little or no interactions with human TfR by DCS (Fig. 2b) and, similarly, no reduction of uptake in TfR-silenced cells (Fig. 2c). Similar results are obtained for analogues of the SiO₂-PEG₈-Tf particles with bovine Tf (SiO₂-PEG₈-bTf in Fig.2e-f).

Uptake of the pegylated particles without functionalization is higher than for Tf-particles, but does not depend on TfR (Fig. 2d and 2f). The actual uptake mechanism of pegylated particles (here as negative controls) is still under discussion³², but overall these results illustrate that the absolute uptake level is of little value in determining the specificity of nanoparticle-cell interactions. Nanoparticle design needs to be optimised in order to achieve recognition by the targeted receptors and approaches such as the one presented can be used to determine whether targeting is achieved.

All the results presented so far are obtained in buffer or serum free medium. A second step is to verify whether targeting is preserved in more realistic biological environments. To probe this question, we have performed similar studies in foetal bovine serum (FBS), though in principle one can use any relevant biological milieu. As serum concentration increases, DCS and immuno dot-blots show that the interaction of the nanoparticles with TfR decreases, ultimately becoming negligible (Fig. 3a-b and Supplementary Fig. S6a). On cells, addition of serum decreases the overall uptake, but, more significantly, the fraction of uptake that depends on TfR also decreases (Fig. 3c and Supplementary Fig. S6b), suggesting that the particles entirely lose their specificity (as illustrated in Fig. 3d). The study in FBS is of interest because endogenous bovine Tf has significantly lower affinity for human TfR, and competes much less with the human Tf-grafted particles. We can confirm that loss of targeting occurs also in human serum (Supplementary Fig. S7-S9). Furthermore, we can eliminate the competition of free Tf, and show that both in Tf-depleted and non-depleted human serum targeting is lost (Supplementary Fig. S9). Tf depletion is repeated until there is no residual Tf, while preserving the general serum composition (Supplementary Fig. S7-8). Collectively these results suggest that, with increasing serum concentration (whether it contains competing free Tf or not) the targeting capacity of Tf-particles is lost.

To further clarify this, nanoparticles are exposed to serum and isolated as described previously³³ to investigate whether there is a contribution of particle-serum binding (termed 'hard corona' because of its durability) in these observations. Indeed, for pegylated and pegylated Tf-functionalized nanoparticles protein binding is observed, though much less than for the non-pegylated particles (Supplementary Fig. S6c and S10).

A range of Tf-functionalized PEG₈-particles further modified with secondary PEG on the particle surface or directly on Tf has also been also prepared, in an attempt at controlling unspecific protein binding (see Supplementary Methods for details). In all cases, however, the targeting specificity is lost upon exposure to biological serum (Supplementary Fig. S11). In conclusion, nanoparticle grafting of targeting molecules (even where the protein remains functional) does not simply imply bio-recognition by corresponding receptors. More significantly, when targeting is achieved in simple dispersions, such as PBS, this can be lost in relevant physiological conditions. Also, besides the absolute uptake, a most critical feature

is the capacity of the nanoparticles to discriminate between different targets, particularly in the complex biological milieu in which they are applied. In practice, failure to achieve this may allow accumulation not only in target cells, but also in cells that do not exhibit any pathology, not intended to be targeted.

In future, it seems necessary to carry out binding and cell-level studies in a variety of biological fluids in which the particles will be applied. Success in similar systems by no means implies success *in vivo*, but if targeting is not observed in relevant fluids, apparent targeting *in vivo* may be a consequence of other poorly understood phenomena. Indeed, we may generalize these comments, beyond the focus of these experiments, since binding to cells or tissue components (rather than uptake) may be sufficient prior to thermal ablation^{34,35} or other therapeutic strategies. Such cases also could benefit from a comparable *in situ* binding analysis as discussed here.

Though these studies focus on a single receptor, the mechanisms involved are of general nature, and suggest the need to mechanistically link ligand-targeting to specific biological outcomes. The approaches outlined here may be of general value in such studies, and possibly shed some light on factors rendering some targeting studies more promising than others⁵⁻⁷.

Methods

Particle Characterization and Differential Centrifugal Sedimentation Detailed methods for particle synthesis are reported in Supplementary Information. Nanoparticle hydrodynamic diameter and zeta potential were measured on a Malvern Nanosizer ZS. Size measurements are averaged results from 3x11 runs at 25 °C. Zeta potential experiments are averaged from 2 runs of between 10 and 100 scans at 25 °C. Differential centrifugal sedimentation (DCS) experiments were performed with a CPS Disc Centrifuge DC24000 (CPS instruments). For the titration, 0.5 mg/ml SiO₂ nanoparticles in phosphate buffer saline (PBS) were incubated with varying concentrations of TfR for 1 hour at room temperature (RT) prior to measurement. A recombinant soluble fragment of the full human TfR, produced from a mouse myeloma cell line (NSO-derived) was used (R&D Systems). This corresponds to the extracellular domain Cys89-Phe760, which has been shown to remain active as a soluble fragment, and includes the Tf-binding region 569-760. In case of the reversed receptor binding, nanoparticles incubated with the receptor were subsequently incubated with excess free Tf (250 µg/ml) for 1 hour at RT, prior measurement. For the measurements in-situ, 0.5 mg/ml SiO₂ nanoparticles were dispersed in 10 % and 55 % serum (in PBS) and incubated with 20 µg/ml TfR for 1 hour at RT. The total volume of injected sample in each run was 0.4 ml.

Immuno Dot-blots

The immuno dot-blots were prepared by spotting mouse monoclonal antibodies against TfR, Tf, or HSA (human serum albumin) (Abcam - ab9179, ab769, ab10241, respectively) on polyvinylidene fluoride (PVDF) membranes (1 μ l at 100, 20 and 10 μ g/ml). The blots were blocked in 5 % skimmed milk in PBS for 1 hour at RT, washed 3 times (10 minutes each) in PBS, and incubated with 0.04 mg/ml nanoparticles in PBS for 1 hour at RT. Blots were washed 3 times for 10 minutes, dried and scanned for fluorescence using TYPHOON 9200 imager.

Cell Culture

Tissue culture reagents were purchased from GIBCO Invitrogen Corporation/Life Technologies Life Sciences (Carlsbad, CA) unless otherwise specified. A549 cells (ATCC-CCL-185) were maintained as monolayer cultures in MEM supplemented with 10% foetal bovine serum (FBS), at 37 °C and 5 % CO₂ (cMEM).

Cell Silencing and Flow Cytometry

20,000 cells were seeded in 12-well plates (Greiner), and incubated for 24 hours prior to silencing of the gene coding for transferrin receptor (TFRC). Then, cells were transfected with 30 pmol of Silencer Select siRNA (Ambion) using Oligofectamine (Invitrogen) according to the manufacturer's instructions. Neg1 silencer was used as a negative control. Cells were transfected with siRNAs for 72 hours in all experiments, prior to exposure to nanoparticles or labelled transferrin.

In order to expose the cell to the nanoparticles, after 72 hour silencing, cells were washed for 10 minutes in serum free MEM. Then the medium was replaced by the nanoparticle dispersions, freshly prepared by diluting the nanoparticle stock in serum free MEM, cMEM or medium supplemented with 55 % FBS, for different times, depending on the experiment. To measure eventual nanoparticle export, after exposure to nanoparticles, the dispersion was discarded and after 3 washes with PBS, nanoparticle-free cMEM medium was added to the cells for further time. Similar experiments were performed by exposing cells to 5 µg/ml Alexa 488 labeled human transferrin (Molecular Probes) in serum free MEM. For flow cytometry, cells were washed thrice with PBS and harvested with trypsin. Cell pellets were then fixed at RT with 4 % formalin (Sigma) for 20 minutes and re-suspended in PBS before cell-associated fluorescence (15,000-50,000 cells per sample) was detected using an Accuri C6 reader (BD Accuri Cytometers). The results are reported as the median of the distribution of cell fluorescence intensity, averaged between 2-3 independent replicates. Error bars are the standard deviation between replicates. Each experiment was performed at least 3 times.

Fluorescence Imaging

For cell fluorescence imaging, A549 cells were grown on 15 mm glass coverslips inside a 12 well plate and silenced as described above. After exposure to nanoparticles, samples were washed with 3 x 1 ml PBS, fixed for 20 min with 4 % formalin, permeabilized for 5 min in 0.1 % saponin from Quillaja bark (Sigma), and incubated for 1 hour at RT with primary mouse monoclonal antibodies (1:100) against the lysosomal-associated membrane protein 1 LAMP1 or TfR (Abcam), for lysosome and transferrin receptor staining respectively. Then, cells were washed with 3 x 1 ml PBS, and incubated at RT for 1 hour with Alexa 647 Goat Anti-mouse IgG (1:400) as a secondary antibody (Molecular Probes). Samples were washed with 3 x 1 ml PBS and incubated for 3 minutes with 4',6-diamidino-2-phenylindole (DAPI,Sigma) before mounting with MOWIOL (Calbiochem) on imaging glass slides. Cells were observed using a Leica DMI6000B epifluorescence microscope or an Olympus FluoView FV1000 confocal microscope. Co-localization of TfR with nanoparticles was analysed using ImageJ software (Colocalization plugin; http://rsb.info.nih.gov/ij/).

References

- 1 Ruoslahti, E., Bhatia, S.N. & Sailor, M.J. Targeting of drugs and nanoparticles to tumors. *J. Cell Biol.* **188**, 759-768 (2010).
- Ferrari, M. Cancer nanotechnology: Opportunities and challenges. *Nature Rev. Cancer* **5**, 161-171 (2005).
- 3 Cedervall, T. et al. Understanding the nanoparticle-protein corona using methods to quantify exchange rates and affinities of proteins for nanoparticles. *Proc. Natl. Acad. Sci. U. S. A.* **104**, 2050-2055 (2007).
- 4 Nel, A.E. et al. Understanding biophysicochemical interactions at the nano-bio interface. *Nature Mater.* **8**, 543-557 (2009).
- Hrkach, J. et al. Preclinical development and clinical translation of a PSMA-targeted docetaxel nanoparticle with a differentiated pharmacological profile. *Sci. Transl. Med.* **4**, 128-139 (2012).
- Davis, M.E. et al. Evidence of RNAi in humans from systemically administered siRNA via targeted nanoparticles. *Nature* **464**, 1067-1070 (2010).
- Keystone, E. et al. Certolizumab pegol plus methotrexate is significantly more effective than placebo plus methotrexate in active rheumatoid arthritis: Findings of a fifty-two–week, phase III, multicenter, randomized, double-blind, placebo-controlled, parallel-group study. *Arthritis Rheum.* **58**, 3319-3329 (2008).

- 8 Ferrari, M. Frontiers in cancer nanomedicine: Directing mass transport through biological barriers. *Trends Biotechnol.* **28**, 181-188 (2010).
- 9 Nie, S., Xing, Y., Kim, G.J. & Simons, J.W. Nanotechnology applications in cancer. *Annu. Rev. Biomed. Eng.* **9**, 257-288 (2007).
- Zamboni, W.C. et al. Best practices in cancer nanotechnology: Perspective from NCI Nanotechnology Alliance. Clin. Cancer Res. 18, 3229-3241 (2012).
- Jain, R.K. & Stylianopoulos, T. Delivering nanomedicine to solid tumors. *Nature Rev. Clin. Oncol.* **7**, 653-664 (2010).
- Moghimi, S.M., Hunter, A.C. & Murray, J.C. Nanomedicine: Current status and future prospects. *FASEB J.* **19**, 311-330 (2005).
- Salvati, A. et al. Experimental and theoretical comparison of intracellular import of polymeric nanoparticles and small molecules: Toward models of uptake kinetics. *Nanomedicine N. B. M.* **7**, 818-826 (2011).
- 14 Iversen, T.-G., Skotland, T. & Sandvig, K. Endocytosis and intracellular transport of nanoparticles: Present knowledge and need for future studies. *Nano Today* 6, 176-185 (2011).
- Mitragotri, S. & Lahann, J. Physical approaches to biomaterial design. *Nature Mater.* **8,** 15-23 (2009).
- Petros, R.A. & DeSimone, J.M. Strategies in the design of nanoparticles for therapeutic applications. *Nature Rev. Drug Discov.* **9,** 615-627 (2010).
- Decuzzi, P. et al. Size and shape effects in the biodistribution of intravascularly injected particles. *J. Controlled Release* **141**, 320-327 (2010).
- Barenholz, Y. Liposome application: Problems and prospects. *Curr. Opin. Colloid Interface Sci.* **6**, 66-77 (2001).
- Farma, J.M. et al. Direct evidence for rapid and selective induction of tumor neovascular permeability by tumor necrosis factor and a novel derivative, colloidal gold bound tumor necrosis factor. *Internatl. J. Cancer* **120**, 2474-2480 (2007).
- Paciotti, G.F. et al. Colloidal gold: A novel nanoparticle vector for tumor directed drug delivery. *Drug Del.* **11,** 169-183 (2004).
- Deng, Z.J. et al. Nanoparticle-induced unfolding of fibrinogen promotes Mac-1 receptor activation and inflammation. *Nature Nanotech.* **6,** 39-44 (2011).
- Wang, J. et al. Soft Interactions at Nanoparticles Alter Protein Function and Conformation in a Size Dependent Manner. *Nano Letters* **11**, 4985-4991 (2011).
- Otsuka, H., Nagasaki, Y. & Kataoka, K. PEGylated nanoparticles for biological and pharmaceutical applications. *Adv. Drug Del. Rev.* **55**, 403-419 (2003).

- Hamad, I. et al. Distinct polymer architecture mediates switching of complement activation pathways at the nanosphere–serum interface: Implications for stealth nanoparticle engineering. *ACS Nano* **4**, 6629-6638 (2010).
- Daniels, T.R., Delgado, T., Helguera, G. & Penichet, M.L. The transferrin receptor part II: Targeted delivery of therapeutic agents into cancer cells. *Clin. Immunol.* **121**, 159-176 (2006).
- Thorstensen, K. & Romslo, I. The role of transferrin in the mechanism of cellular iron uptake. *Biochem. J.* **271**, 1-10 (1990).
- 27 Kumar, R. et al. Covalently dye-linked, surface-controlled, and bioconjugated organically modified silica nanoparticles as targeted probes for optical imaging. *ACS Nano* **2**, 449-456 (2008).
- Högemann-Savellano, D. et al. The transferrin receptor: a potential molecular imaging marker for human cancer. *Neoplasia* **5**, 495-506 (2003).
- Qian, J. et al. Bio-molecule-conjugated fluorescent organically modified silica nanoparticles as optical probes for cancer cell imaging. *Opt. Express* **16**, 19568-19578 (2008).
- Wu, J., Ye, Z., Wang, G. & Yuan, J. Multifunctional nanoparticles possessing magnetic, long-lived fluorescence and bio-affinity properties for time-resolved fluorescence cell imaging. *Talanta* **72**, 1693-1697 (2007).
- Kim, J.A., Aberg, C., Salvati, A. & Dawson, K.A. Role of cell cycle on the cellular uptake and dilution of nanoparticles in a cell population. *Nature Nanotech.* **7**, 62-68 (2012).
- Shibuya-Fujiwara, N. et al. Phagocytosis in vitro of polyethylene glycol-modified liposome-encapsulated hemoglobin by human peripheral blood monocytes plus macrophages through scavenger receptors. *Life Sci.* **70**, 291-300 (2001).
- 33 Walczyk, D. et al. What the cell "sees" in bionanoscience. *J. Am. Chem. Soc.* **132,** 5761-5768 (2010).
- 34 Chakravarty, P. et al. Thermal ablation of tumor cells with antibody-functionalized single-walled carbon nanotubes. *Proc. Natl. Acad. Sci. U. S. A.* **105**, 8697-8702 (2008).
- Hirsch, L.R. et al. Nanoshell-mediated near-infrared thermal therapy of tumors under magnetic resonance guidance. *Proc. Natl. Acad. Sci. U. S. A.* 100, 13549-13554 (2003).

Acknowledgements

Funding for the project has been generously provided by the INSPIRE (Integrated NanoScience Platform for Ireland) programme, funded by the Irish Government's Programme for Research in Third Level Institutions, Cycle 4, National Development Plan 2007-2013, the Irish Research Council for Science, Engineering and Technology, the Helmholtz-Gemeinschaft Deutscher Forschungszentren e. V. Virtual Institute grant Nano Tracking (Agreement number VH-VI-421), and Science Foundation Ireland (09/RFP/MTR2425), and is based upon work supported by the Small Collaborative projects NeuroNano (NNP4-SL-2008-214547) and NanoTransKinetics (NMP4-2010-EU-US-266737), as well as the project 3micron (NMP-2009-LARGE-3-246479), funded by the European Commission 7th Framework Programme. The ESF Research Networking Programme EpitopeMap is also gratefully acknowledged. Use of the Conway Institute Flow Cytometry and Imaging Facilities and the Biological Imaging suite (University College Dublin) is acknowledged. Jeremy C. Simpson is acknowledged for assistance with RNA interference experiments.

Additional Information

Supplementary information accompanies this paper at www.nature.com/naturenanotechnology. Reprints and permission information is available online at http://npg.nature.com/reprintsandpermissions/.

Correspondence and requests for materials should be addressed to K.A.D. and E.M.

Author Contributions

A.S.P. performed experiment on cells, analysed and interpreted the data and wrote the paper. A.S.P. performed biological interaction experiments, analysed and interpreted the data and contributed to the writing of the paper. E.M. performed synthesis and characterization of nanoparticles, analysed and interpreted the data and wrote the paper. M.P.M. prepared and characterised the depleted serum, analysed and interpreted the data and contributed to the writing of the paper. K.P. contributed to silencing and competition experiments and D.R.H. and P.M.K. contributed to the synthesis and characterization of the particles. F.B.B. and C.Å. analysed and interpreted the data and contributed to the writing of the paper. K.A.D. conceived and designed the experiments, analysed and interpreted the data and wrote the paper.

Competing Financial Interests Statement

The authors have no competing interests as defined by Nature Publishing Group, or other interests that might be perceived to influence the results and/or discussion reported in this article.

Figures and Table

Scheme 1. Nanoparticle synthesis scheme. a) Direct coupling approach: grafting of transferrin (Tf) on silica-COOH nanoparticles by EDAC chemistry. b) Preparation of pegylated Tf particles. Tf is modified with PEG linkers of different lengths (X) to introduce a reactive thiol to the protein. Silica nanoparticle surfaces are initially aminated using APTMS. The aminated particles are then reacted with NHS-PEG-Mal of different lengths (Y), and the SATPEG modified Tf is subsequently "clicked" by the thiol-maleimide reaction at the particle surface to prepare different nanobioconjugates. The configuration with X= 4 and Y = 8 (SiO₂-PEG₈-Tf) showed bio-recognition by TfR.

Figure 1. Interaction of functional pegylated human transferrin particles (SiO₂-PEG₈-Tf) with soluble Tf receptor (TfR) and uptake in A549 cells. a and b) Apparent diameter obtained by DCS for 0.5 mg/ml SiO₂-PEG₈-Tf nanoparticles incubated with increasing amount of TfR. The shift of the weight distribution maximum indicates binding of TfR to the active Tf binding sites of the functionalized Tf-nanoparticles, as showed in the scheme on the right. The titration shows saturation of Tf-NP binding sites at increasing TfR concentration. c-e) A549 cells are silenced for 72 hours as described in the Methods with a negative silencer control (neg siRNA) and for TfR (siTFRC), prior to exposure to nanoparticles (50 µg/ml) in serum free MEM. c) Confocal images (overlapped and single channels) of control A549 cells confirm that some of the nanoparticles (green) colocalize with TfR (red) (5 hour exposure. Blue: DAPI stained nuclei. Scale bar: 10 µm) In white: colocalization of nanoparticles with TfR (see Methods for details). d) The median cell fluorescence intensity obtained by flow cytometry from A549 cells exposed to different concentrations of SiO₂-PEG₈-Tf shows that the uptake is strongly reduced in cells silenced for TfR. Fluorescence microscopy (below) on control (neg siRNA) and silenced (siTFRC) A549 cells (~7 hours exposure. Blue: DAPI stained nuclei. Scale bar: 10 μm) confirms that in cells silenced for TfR uptake is strongly reduced, however some nanoparticles enter by other (non-TfR) pathways. e) Median cell fluorescence intensity obtained by flow cytometry from A549 cells exposed for 1 and 4 hours to SiO₂-PEG₈-Tf, followed by particle removal and incubation with nanoparticle-free complete MEM (cMEM) for further hours. The cell fluorescence intensity does not decrease and this suggests no significant export for these nanoparticles. Confocal imaging on A549 cells after 5 hours exposure shows that the

internalized nanoparticles (green) accumulate in the lysosomes (red). Blue: DAPI stained nuclei. Scale bar: 10 μm.

Figure 2. Interaction of surface grafted human transferrin particles (SiO₂-Tf), pegylated and pegylated bovine transferrin particles (SiO₂-PEG₈ and SiO₂-PEG₈-bTf) with soluble Tf receptor (TfR) and A549 cells. a) Schematic representation of SiO₂ nanoparticles directly grafted with human Tf. b, d and e) Apparent diameter obtained by DCS for 0.5 mg/ml nanoparticles incubated with 20 μg/ml of TfR. c and f) A549 cells are silenced for 72 hours as described in the Methods with a negative silencer control (neg siRNA) and for TfR (siTFRC), prior to exposure to nanoparticles. Median cell fluorescence intensity obtained by flow cytometry from A549 cells exposed to 50 µg/ml nanoparticles in serum free MEM. For surface grafted human Tf particles (b), DCS shows only a very small shift of the weight distribution maximum, indicating minimal binding of the receptor to the active Tf binding sites of the functionalized Tf-nanoparticles. This is reflected also on cells (c), where even though internalization is very high, only a small reduction of uptake is observed after silencing, suggesting a minor role of TfR for the uptake of these particles. For pegylated (d) and pegylated bovine Tf particles (e), DCS shows no shift of the weight distribution maximum, indicating no significant TfR binding. Similarly on cells (f), no reduction of uptake is observed after silencing, suggesting that the uptake of these particles is not mediated by TfR.

Figure 3. *In-situ* targeting of SiO₂-PEG₈-Tf nanoparticles with soluble Tf receptor and uptake in A549 in presence of serum. a) DCS assessment of TfR binding to pegylated human Tf particles in the presence of bovine serum. A reduction of the apparent diameter is observed at increasing amount of serum, indicating loss of TfR binding when a protein corona is formed on the NP surface, "shielding" the active binding sites from recognition by TfR. The apparent diameter of bare nanoparticles and nanoparticles incubated with TfR in PBS is shown as reference. Below, immunological detection of SiO₂-PEG₈-Tf/TfR complexes, with use of anti-TfR antibody (1 μl 100, 20 and 10 μg/ml from left to right). The dot blot confirms the reduction of TfR binding at increasing bovine serum content. b) Schematic representation of blocked Tf-TfR interaction in presence of bovine serum proteins. c) A549 cells are silenced for 72 hours as described in the Methods with a negative silencer control (neg siRNA) and for the transferrin receptor (siTFRC), prior to exposure to nanoparticles. Median cell fluorescence intensity obtained by flow cytometry from A549 cells exposed to 50 μg/ml pegylated human Tf particles (SiO₂-PEG₈-Tf) in serum free MEM (0%), complete medium (10%) and MEM supplemented with 55% serum (55%). As shown in Fig.

1d, the uptake is strongly reduced in cells silenced for TfR. However at increasing serum content the uptake decreases and the effect of TfR is also lost. d) Schematic representation of loss of TfR targeting for Tf-conjugated nanoparticles in the presence of bovine serum proteins (Endogenous Tf, where present, could also compete for TfR).

Table 1. Physico-chemical characterization of typical batches of bare and functionalized SiO₂ nanoparticles. The size and zeta potential of the bare and functionalized silica nanoparticles in PBS have been measured using a Malvern Nanosizer. The amount of grafted Tf has been quantified by BCA Microassay (see Methods for details).

Sample	D _H ^a in PBS [nm]	PDI ^b	Zeta potential [mV] (pH 6.8, I=0.1M)	Tf [μg/mg NP]
SiO ₂	65	0.07	-15	-
SiO ₂ -PEG ₈	74	0.09	-23	-
SiO ₂ -PEG ₈ -Tf	86	0.06	-4	112
SiO ₂ -PEG ₈ -bTf	88	0.09	-4	109

Note: DLS, being an average, for such complex systems (especially in more complex media, see Table S1) may be less reliable than the distributions of monomers, dimers, and aggregates derived from DCS (see for example Fig.1a, 3a and Supplementary Figures).

- a. Z-average hydrodynamic diameter extracted by cumulant analysis of the data.
- b. Polydispersity Index from cumulant fitting.